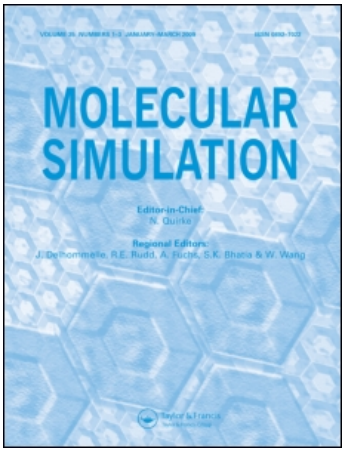

Molecular Simulation
Publication details, including instructions for authors and subscription information:
http://www.informaworld.com/smpp/title~content=t713644482

Molecular dynamics of nanoparticle translocation at lipid interfaces

M. Schneemilch[a]; N. Quirke[a]
[a] Department of Chemistry, Imperial College London, London, UK

Online publication date: 15 October 2010

To cite this Article Schneemilch, M. and Quirke, N.(2010) 'Molecular dynamics of nanoparticle translocation at lipid interfaces', Molecular Simulation, 36: 11, 831 — 835
To link to this Article: DOI: 10.1080/08927021003775433
URL: http://dx.doi.org/10.1080/08927021003775433

Molecular Simulation
Vol. 36, No. 11, September 2010, 831–835

Taylor & Francis
Taylor & Francis Group

Molecular dynamics of nanoparticle translocation at lipid interfaces

M. Schneemilch and N. Quirke*

Department of Chemistry, Imperial College London, London NW7 2AY, UK

(*Received 15 March 2010*; *final version received 15 March 2010*)

We report molecular dynamics simulations of bare and hydrophilic C60 nanoparticles at a dipalmitoylphosphatidylcholine–water interface representing a model lung surfactant layer. Bare C60 particles penetrate into the lipid layer from the vapour to sit just before the lipid head groups while hydrophilic nanoparticles penetrate into the head-group–water interface. The potential of mean force shows how the preferred position varies with the density of the lipid layer (in the physiological range) and with hydrophilicity. We conclude that C60 nanoparticles will not spontaneously diffuse across a surfactant monolayer but that functionalised nanoparticles may, depending on the membrane density, translocate the membrane to reach the water phase in 10–20 ns.

Keywords: nanoparticles; lung; translocation; lipids

1. Introduction

There is a long history of disease caused by inhaled particles [1]. Recently, environmental ultrafine particles, with aerodynamic diameters < 100 nm (i.e. nanoparticles), have been recognised as a serious health problem [2–4]. In susceptible subjects with existing heart and lung disease, there is an increased risk of morbidity and mortality [2,5]. Some of these effects are attributed to translocated nanoparticles based on their potential effects on vascular function [6,7].

Fullerene-like structures are present in diesel soot [8] and graphitic polyhedral carbon particles [9], comparable with those generated by arc discharge, exist in petrol soot. Nanoparticles may exist as singlet particles or as aggregates [10]. For singlet particles, there is good evidence that particles with aerodynamic diameters down to 10 nm deposit readily, largely by diffusion, in the airways and centriacinar, respiratory regions of the lung [11]. Those less than 10 nm are found preferentially in the upper airways [12]. Despite many studies, the exact nature of nanoparticle interaction with lung lining fluids, their transport into and across biological membranes remains a mystery [13]. In this paper, we report new simulation results elucidating the translocation of fullerene particles across model lung surfactant barriers.

Previous simulations conducted by Qiao et al. [14] have shown that pristine C60 molecules in solution will spontaneously enter the hydrophobic tail region of a lipid bilayer and that functionalised nanoparticles will spontaneously translocate from a lipid bilayer to the aqueous phase. However, unlike the case of the bilayer, the specific area of the *monolayer* changes during the course of the breathing cycle, which would be expected to change the resistance to nanoparticle translocation. Indeed, it was found in the course of this investigation that a reduction in the specific area restricts the movement of nanoparticles in the interfacial region. We also show that there is a significant energy barrier that can prevent even functionalised nanoparticles from migrating from the interface into the bulk water.

Lung surfactant forms a film at the air–liquid interface that controls surface tension during breathing [15]. The surfactant is composed of two main fractions: 90% lipids (phospholipids 80% and neutral lipids 10%) and 10% surfactant-specific proteins. Phosphatidylcholine (PC) forms 70–80% of the phospholipid of which 50–70% is saturated, especially as dipalmitoylphosphatidylcholine (DPPC). Another significant component is cholesterol. It is possible that this process may be mediated by one of the proteins present in lung surfactant but in this first report we consider a pure DPPC monolayer.

Nanoparticles were introduced to two monolayers of different specific areas. The first has a specific area of 64 A^2 per lipid (ApL), which is identical to that found for the bilayer in the absence of surface tension. The second has a lower specific area of 57 ApL that places it in the liquid expanded (LE) region of the phase diagram. Of particular interest are the details of the entry of the nanoparticles into the hydrophobic tail region of the monolayer, the position of the particle relative to the lipid–water interface and the free energy barrier for translocation of the nanoparticle.

Aside from the risk posed by nanoparticles, they also offer the possibility of beneficial medical applications such as targeted drug delivery, and a detailed understanding of their interaction with biological systems is

*Corresponding author. Email: n.quirke@ic.ac.uk

ISSN 0892-7022 print/ISSN 1029-0435 online

DOI: 10.1080/08927021003775433
http://www.informaworld.com

vital for this purpose. Our final goal is therefore to gain a better understanding of the processes that govern the transport of engineered nanoparticles into the human body with the hope that this effort sheds some light on the real impact that such nanoparticles might have on human health, both adverse and beneficent.

2. Simulation details

In this preliminary investigation, we use a simple model of the functional lung lining membrane comprising only DPPC lipids. All simulations were performed in the NVT ensemble using GROMACS [16,17] at a physiological temperature of 310 K. The DPPC and SPC/E molecules were coupled separately to a Berendsen thermostat [18] and the nanoparticles were uncoupled. Lennard-Jones potentials were cut off at 1 nm and particle mesh Ewald summation (PME) [19] was used to calculate the electrostatic forces.

The lipid–water system contained 128 DPPC molecules and 3655 water molecules. The initial configuration was based on the popular bilayer configuration published by Wong-Ekkabut et al. [20]. The bilayer was inverted and vacuum introduced to obtain two monolayer leaflets in the *xy* plane, each comprising 64 lipids with a specific area of 64 ApL. The DPPC force field has been tested rigorously [21]. The water model was SPC/E. The C60–lipid tail interaction was based on Werder et al. [22].

After inversion, the monolayers were allowed to equilibrate for 10 ns. An additional set of monolayers with a specific area of 57 ApL was generated by applying a series of compression steps to the original system. During each compression step, a lateral force was applied until the specific area decreased by 1 ApL, at which point a equilibration step was performed before application of the next compression step.

Functionalised nanoparticles were generated by adding hydroxyl groups at randomly chosen sites on the C60 molecule. In particular, functionalised nanoparticles with 20 OH groups were the focus of study. All angles in the nanoparticle were fixed, as a result only the hydrogen atoms were able to move in relation to the rest of the molecule. The various interactions are therefore identical to those used by Qiao except that here the SPC/E model was used.

Two types of simulation were performed using two nanoparticles, one for each monolayer in the system (see the inserts in Figure 1). In the first one, the nanoparticles were allowed to enter the monolayers starting from rest approximately 1.5 nm from each respective interface in the gas phase. These simulations were run for 100 ns. After 50 ns, data were collected to calculate structure factors, lateral diffusion coefficients and monolayer density profiles. In addition, potential of mean force (PMF) simulations were conducted on pristine nanoparticles and those with 20 OH groups. Two separate simulations of this type were run on each system.

The PMF was calculated using a similar procedure to Qiao et al. [14]. The nanoparticles were held fixed at various positions in their respective monolayers and the force acting on each molecule calculated. At each point, the system was equilibrated for 3 ns and the forces calculated over a period of 4 ns. The PMF was calculated by integrating the measured force, which was averaged over both nanoparticles. These forces will be representative of the local environment during the translocation event but may not reflect the long-time equilibrium results, for example, in the water phase where surfactant pushed out of the layer by the nanoparticle may, over long times, rejoin the layer.

3. Results

The 64 ApL system will be discussed first, as the results may be compared to those for the bilayer system where each leaflet adopts this specific area. Sample trajectories of the *z*-coordinate of the centre of mass of each nanoparticle are plotted in Figure 1. The blue trajectory shows the path of the pristine nanoparticle while the trajectory of the C60 molecule functionalised with 20 OH groups is shown in red. The boundaries of the lipid layer are denoted by the horizontal lines, which correspond to the peak of the lipid number density for the lipid–water interface and the vanishing point of the lipid number density for the lipid–

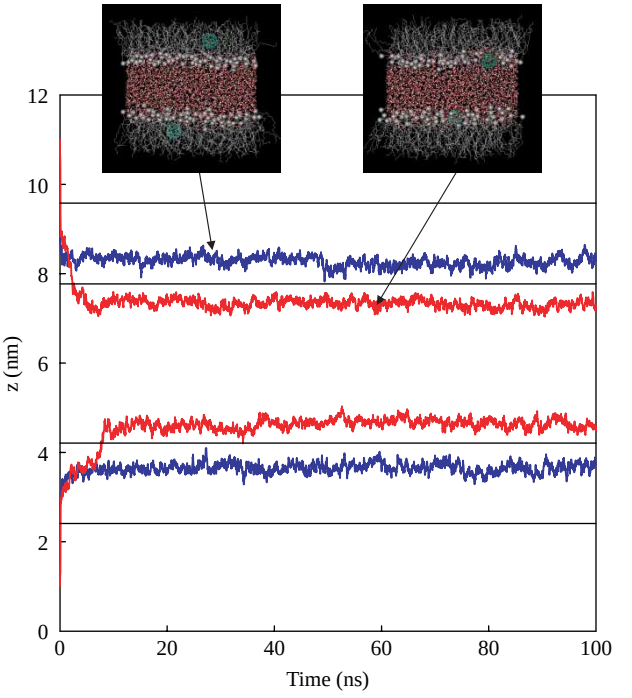

Figure 1. The *z*-position of the nanoparticles in the 64 ApL monolayer. The horizontal lines denote the interfaces of each leaflet. The water–lipid interface is located at the peak of the lipid number density and the lipid–vacuum interface is located at the point at which the lipid number density falls to zero. Blue, pristine C60 molecule; red, C60 molecule functionalised with 20 OH groups.

vacuum interface. The functionalised nanoparticle readily translocates to the lipid–water interface but remains in the vicinity of the head-group region for the extent of the simulation. The bare nanoparticle, on the other hand, remains inside the lipid tail region. Similar behaviour was observed in the additional runs.

The pristine nanoparticle adopts an equilibrium position approximately 0.5 nm from the lipid–water interface. This agrees with the observations by Qiao et al. [14], who found that a pristine nanoparticle released in the water phase would spontaneously translocate the lipid interface and adopt a similar position within the lipid tail region. They also observed that a C60 molecule functionalised with 20 hydroxyls diffused onto the lipid bilayer but remained on the membrane and did not move into the bilayer. The equilibrium position was approximately 0.5 nm from the interface in the water phase. So that, in this respect, the individual monolayer leaflets behave in a similar fashion to the leaflets in the bilayer when at the same specific area. The surface tension of the monolayer does not change appreciably in response to the addition of the nanoparticle.

Similar data are presented in Figure 2 for the 57 ApL monolayer. Here, the functionalised and pristine nanoparticles remain within the lipid tail region. The functionalised particles approach the water–lipid interface more slowly and do not readily translocate, although the functionalised nanoparticle in the bottom layer does approach the interface closely towards the end of the simulation.

The nanoparticles in the 64 ApL monolayer take approximately 10 ns to reach their respective equilibrium positions, while the figure is roughly 20 ns in the 57 ApL monolayer. This difference is presumably due to steric effects arising from the higher lipid chain density in the 57 ApL monolayer.

These observations can be understood by the examination of the PMF diagrams in Figure 3. They show the PMF as a function of distance from the water–lipid interface, as defined by the peak in the lipid number density. This corresponds to the origin on the ordinate axis; the lipid chains extend towards the positive side of the axis and the water phase to the negative.

In the case of the pristine nanoparticles, the global minimum lies within the lipid tail region. For the 64 ApL system the minimum is roughly 0.5 nm from the interface, while it is 1 nm in the 57 ApL system.

When functionalised, the minimum is significantly lower in the 64 ApL system and lies just inside the water phase. In the 57 ApL system, the position of the global minimum does not change significantly from that for the pristine nanoparticle; however, there is now a second local minimum just inside the water phase. The energy barrier preventing translocation in this system is of the order of 10 k_BT. Of the four separate trajectories obtained for this system, only in one case did the functionalised nanoparticle translocate the water–lipid interface. Based on some

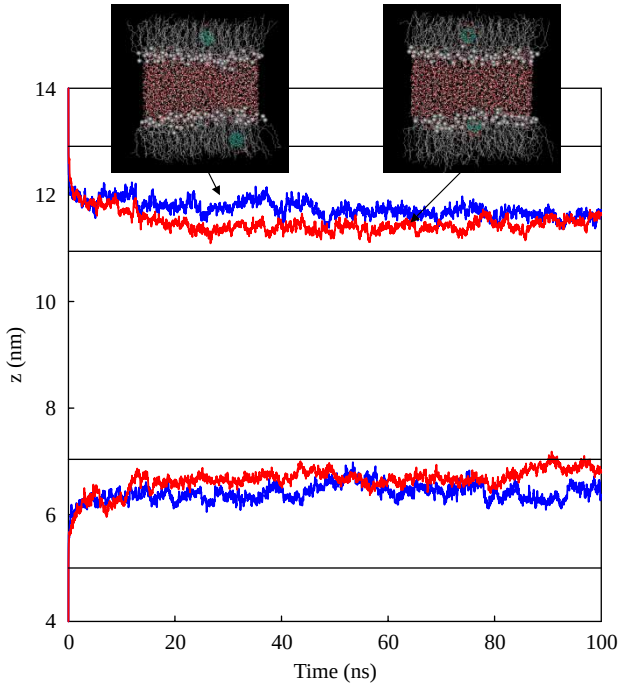

Figure 2. The z-position of the nanoparticles in the 57 ApL monolayer. The horizontal lines denote the interfaces of each leaflet. The water–lipid interface is located at the peak of the lipid number density and the lipid–vacuum interface is located at the point at which the lipid number density falls to zero. Blue, pristine C60 molecule; red, C60 molecule functionalised with 20 OH groups.

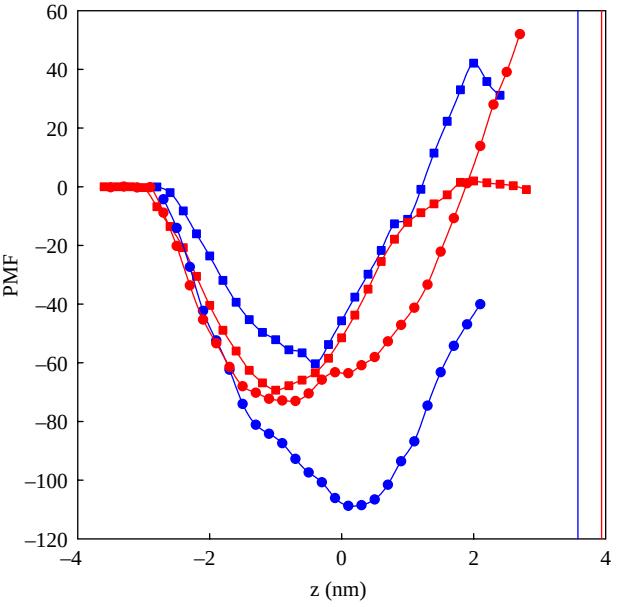

Figure 3. PMF for each system. The origin of the abscissa axis corresponds to the first water–lipid interface. The vertical lines denote the position of the other interface for each system. Blue, 64 ApL; red, 57 ApL; square, C60 molecule; circle, C60 molecule functionalised with 20 OH groups (colour online).

preliminary simulations not reported here, it appears that this functionalisation effect becomes apparent when more than 10 OH groups are added to the C60 molecule.

Once the nanoparticles had passed through the interface during the course of the PMF simulations, they tended to entrain the lipid chains in the immediate proximity. These soon detached from the pristine nanoparticles, which is evident in the sudden inflection of the PMF functions. The functionalised nanoparticles retained the lipids across the full extent of the water phase. In a larger system, it is entirely possible they would have completely removed the lipids from the monolayer.

The lateral diffusivity of the pristine nanoparticle in the 64 ApL monolayer was only $2.7 \pm 0.1 \times 10^{-4}\,\mathrm{nm^2\,ps^{-1}}$. This compares with $3.2 \pm 0.5 \times 10^{-3}\,\mathrm{nm^2\,ps^{-1}}$ for the pristine nanoparticle in the 57 ApL system. The difference presumably arises not from the specific area of the monolayer but from the relative equilibrium position of the nanoparticles, which, in the 64ApL case, lies closer to the lipid–water interface.

When the nanoparticles were functionalised with 20 OH groups, the lateral diffusivity in the 64 ApL system was much higher, $7.8 \pm 0.6 \times 10^{-2}\,\mathrm{nm^2\,ps^{-1}}$. The nanoparticle was more mobile as it was effectively free from the lipid chain region. The lateral diffusivity in the 57 ApL system was $5.2 \pm 1.2 \times 10^{-3}\,\mathrm{nm^2\,ps^{-1}}$. This value is similar to the pristine nanoparticle, a reflection of its similar relative position.

In order to gauge the effect of the nanoparticle on the surrounding lipids, the lipid density and structure factors were calculated as a function of the lateral distance from the centre of the C60 molecule. Each configuration was divided into cylindrical bins of identical area centred on the instantaneous position of the nanoparticle. Time averages of the lipid specific area in each bin and order factors for the 64 ApL system are shown in Figure 4. Note that each chain was considered individually, and assigned to its bin based on the centre of mass of the individual chain.

The pristine nanoparticle tended to harbour a larger number of chains in its immediate lateral vicinity, reflected in the specific area slightly lower than the pure monolayer. These chains had a higher structure factor than the bulk, indicating that these chains were more upright as they wrapped around the nanoparticle. The hydroxylated nanoparticle, on the other hand, tended to displace more chains from its immediate vicinity owing to its greater cross-sectional area and proximity to the head-group region. The chains in the proximity tended to orient slightly more parallel to the surface than the bulk, although the nanoparticle had translocated the lipid chain region.

The situation is somewhat different with the 57 ApL monolayer (Figure 5). The functionalised nanoparticle

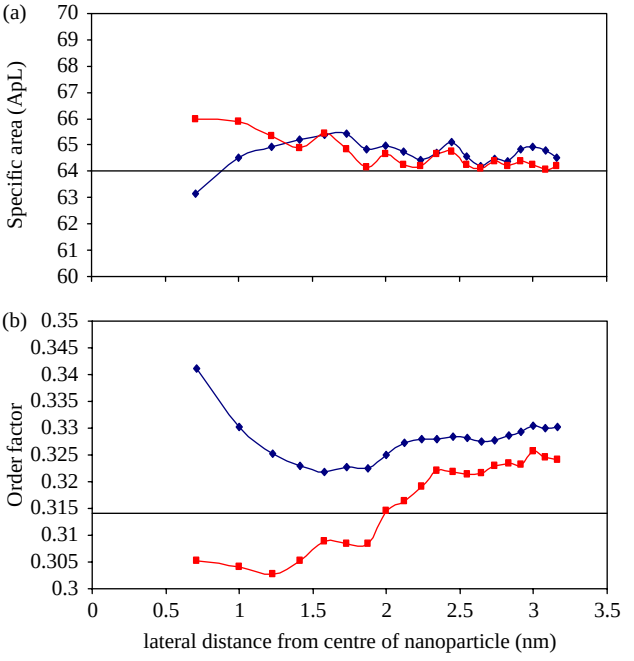

Figure 4. The structure of the 64 ApL monolayer as a function of the lateral distance from the centre of the nanoparticle. (a) The lipid specific area. (b) The structure factor. Time averages are constructed over the period from 50 to 100 ns. The solid lines indicate the average value in the pure lipid monolayer. Blue, pristine C60 molecule; red, C60 molecule functionalised with 20 OH groups (colour online).

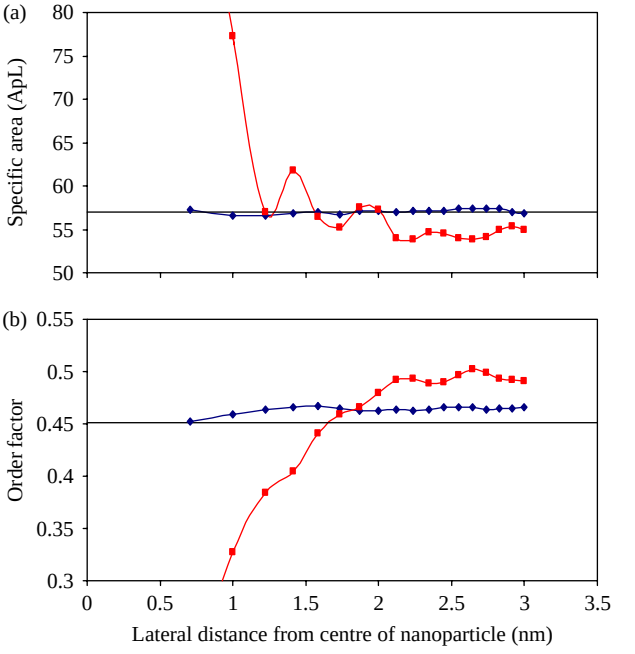

Figure 5. The structure of the 57 ApL monolayer as a function of the lateral distance from the centre of the nanoparticle. (a) The lipid specific area. (b) The structure factor. Time averages are constructed over the period from 50 to 100 ns. The solid lines indicate the average value in the pure lipid monolayer. Blue, pristine C60 molecule; red, C60 molecule functionalised with 20 OH groups (colour online).

displaces the majority of the chains from the immediate vicinity, resulting in a lower specific area in the rest of the cell. Any chains remaining in the area are aligned parallel to the interface. The chains in the rest of the cell are forced into an upright orientation.

In a physiological system, salt will be present in the water phase. There is some evidence from AFM measurements on bilayers [23] that the ions bind the surfactant head groups increasing the mechanical strength of the membrane, decreasing the head-group–head-group distance by approximately 5%. We would therefore expect the presence of salts to decrease the effective head-group area per molecule by $\sim 10\%$ so that the larger head-group area monolayers (64 ApL) would behave more like the lower head-group area case (57 ApL) reported here.

From the current molecular dynamics simulations, it appears that C60 nanoparticles will not spontaneously diffuse across a surfactant monolayer but that functionalised nanoparticles may translocate the membrane to reach the water phase in approximately 10–20 ns.

References

[1] W.K.C. Morgan and A. Seaton, *Occupational Lung Diseases*, Philadelphia, PA, Saunders, 1995.

[2] J. Schwartz, *Is there harvesting in the association of airborne particles with daily deaths and hospital admissions?* Epidemiology 12 (2001), pp. 55–61.

[3] K. Donaldson, V. Stone, A. Clouter, L. Renwick, and W. MacNee, *Ultrafine particles*, Occup. Environ. Med. 58 (2001), p. 211–216.

[4] J. Kaiser, *How dirty air hurts the heart,* Science 307 (2005), pp. 1858–1859.

[5] *Nanoscience and nanotechnologies: Opportunities and uncertainties*, Report of the Working Party of the Royal Society and the Royal Academy of Engineering, July 2004. Available at: http://www.nanotec.org.uk/finalReport.htm.

[6] K. Bagate, J.J. Meiring, M.E. Gerlofs-Nijland, R. Vincent, F. Cassee, and P.J.A. Borm, *Signal transduction pathways involved in particulate matter induced relaxation in rat aorta—spontaneous hypertensive versus Wistar Kyoto rats,* Toxicol. Appl. Pharmacol. 197 (2004), pp. 29–39.

[7] T.R. Nurkiewicz, D.W. Porter, M. Barger, V. Castranova, and M.A. Boegehold, *Particulate matter exposure impairs systemic microvascular endothelium-dependent dilation,* Environ. Health Perspect. 112 (2004), pp. 1299–1306.

[8] T. Ishiguro, Y. Takatori, and K. Akihama, *Microstructure of diesel soot particles probed by electron microscopy: First observation of inner core and outer shell,* Combust. Flame 108 (1997), pp. 231–234.

[9] T.H. Lee, N. Yao, T.J. Chen, and W.K. Hsu, *Fullerene-Iike carbon particles in petrol soot,* Carbon 40 (2002), pp. 2274–2279.

[10] K. Donaldson, V. Stone, A. Clouter, L. Renwick, and W. MacNee, *Ultrafine particles,* Occup. Environ. Med. 58 (2001), pp. 211–216.

[11] H.C. Yeh, B.A. Muggenburg, and J.R. Harkema, In vivo *deposition of inhaled ultrafine particles in the respiratory tract of rhesus monkeys,* Aerosol Sci. Technol. 27 (1997), pp. 465–470.

[12] L. Zhao, S.-S. Feng, and M.L. Go, *Investigation of molecular interactions between paclitaxel and DPPC by langmuir film balance and differential scanning calorimetry,* J. Pharm. Sci. 93 (2004), pp. 86–98.

[13] M. Kendall, T.D. Tetley, E. Wigzell, B. Hutton, M. Nieuwenhuijsen, and P. Luckham, *Lung lining liquid modifies PM2.5 in favor of particle aggregation: a protective mechanism,* Amer. J. Physiol. Lung Cell Mol. Physiol. L109 (2002), p. 282.

[14] R. Qiao, A.P. Roberts, A.S. Mount, S.J. Klaine, and P.C. Ke, *Translocation of C_{60} and its derivatives across a lipid bllayer,* Nano Lett. 7 (2006), pp. 614–619.

[15] L.A.J.M. Creuwels, L.M.G. van Golde, and H.P. Haagsman, *The pulmonary surfactant system: Biochemical and clinical aspects,* Lung 175 (1997), pp. 1–39.

[16] E. Lindahl, B. Hess, and D. van der Spoel, *GROMACS 3.0: A package for molecular simulation and trajectory analysis,* J. Mol. Model. 7 (2001), pp. 306–317.

[17] H.J.C. Berendsen, D. van der Spoel, and R. van Drunen, *GROMACS: A message-passing parallel molecular dynamics implementation,* Comput. Phys. Commun. 91 (1995), pp. 43–56.

[18] H.J.C. Berendsen, J.P.M. Postma, W.F. Van Gunsteren, A. Dinola, and J.R. Haak, *Molecular dynamics with coupling to an external bath,* J. Chem. Phys. 81 (1984), pp. 3684–3690.

[19] T. Darden, L. Perera, L. Li, and L. Pedersen, *New tricks for modelers from the crystallography toolkit: The particle mesh Ewald algorithm and its use in nucleic acid simulations,* Structure 7 (1999), pp. 55–60.

[20] J. Wong-Ekkabut, S. Baoukina, W. Triampo, I.-M. Tang, D. Tieleman and L. Monticelli, *Computer simulation study of fullerene translocation through lipid membranes*, Nature Nanotech. 3 (2008), pp. 363–368

[21] D.P. Tieleman and H.J.C. Berendsen, *Molecular dynamics simulations of a fully hydrated dipalmitoylphosphatidylcholine bilayer with different macroscopic boundary conditions and parameters,* J. Chem. Phys. 105 (1996), pp. 4871–4880.

[22] T. Werder, J.H. Walther, R.L. Jaffe, T. Halicioglu, and P. Koumoutsakos, *On the water–carbon interaction for use in molecular dynamics simulations of graphite and carbon nanotubes,* J. Phys. Chem. B 107 (2003), pp. 1345–1352.

[23] T. Fukuma, M.J. Higgins, and S.P. Jarvis, *Direct imaging of lipid-ion network formation under physiological conditions by frequency modulation atomic force microscopy,* Phys. Rev. Lett. 98 (2007), 106101.